Electroweak results from HERA

A.F.Żarnecki

Faculty of Physics, University of Warsaw

for

Rencontres de Moriond EW 2013

Outline

- Introduction
  - HERA experiments and collected data

Outline

- Introduction
  - HERA experiments and collected data
- Deep Inelastic $e^{\pm}p$ Scattering
  - Measurement of high Q^2 NC and CC DIS
  - Polarization and charge asymmetries
  - Electroweak couplings
  - Contact Interactions

Outline

- Introduction
  - HERA experiments and collected data
- Deep Inelastic $e^{\pm}p$ Scattering
  - Measurement of high Q^2 NC and CC DIS
  - Polarization and charge asymmetries
  - Electroweak couplings
  - Contact Interactions
- Electroweak cross-sections
  - $W^{\pm}$ production
  - Z° production
  - Search for anomalous single t production

Outline

- Introduction
  - HERA experiments and collected data
- Deep Inelastic $e^{\pm}p$ Scattering
  - Measurement of high Q^2 NC and CC DIS
  - Polarization and charge asymmetries
  - Electroweak couplings
  - Contact Interactions
- Electroweak cross-sections
  - $W^{\pm}$ production
  - Z° production
  - Search for anomalous single t production
- Conclusions

Introduction

HERA
electron(positron)-proton collider at DESY

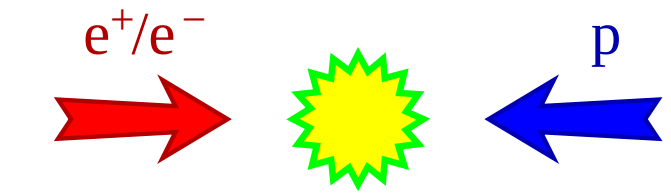

1994−1997
1998−2007

HERA I 1994-2000
about 100pb^{-1} collected per experiment
mainly e^+p data

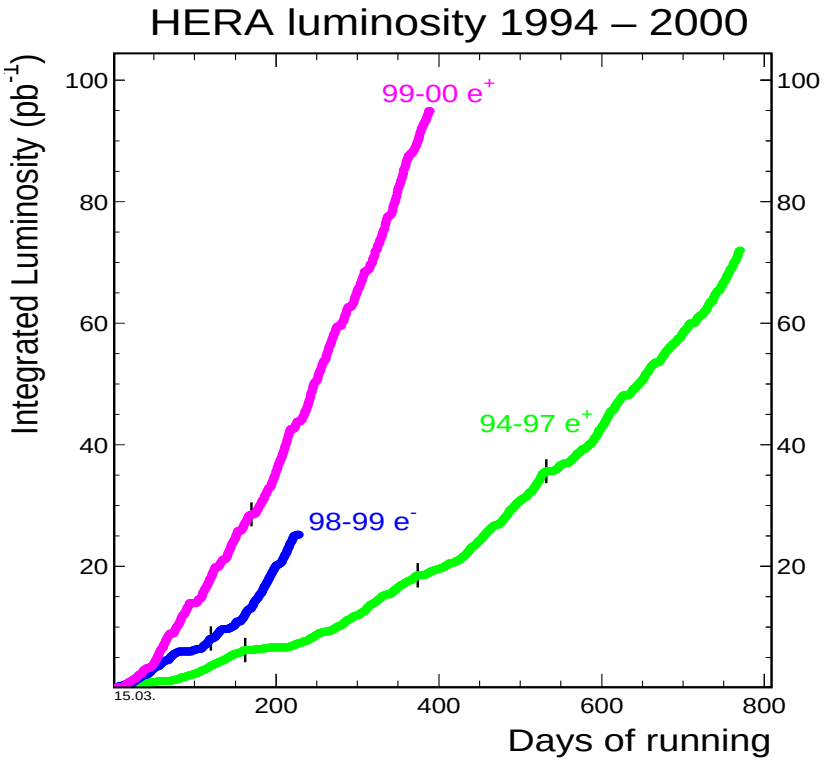

Introduction

HERA
electron(positron)-proton collider at DESY

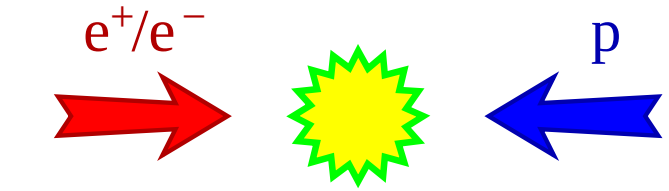

HERA I 1994-2000
about 100pb^{-1} collected per experiment
mainly e^+p data

HERA II 2002-2007
about 400pb^{-1} per experiment
similar amount of e^-p and e^+p data

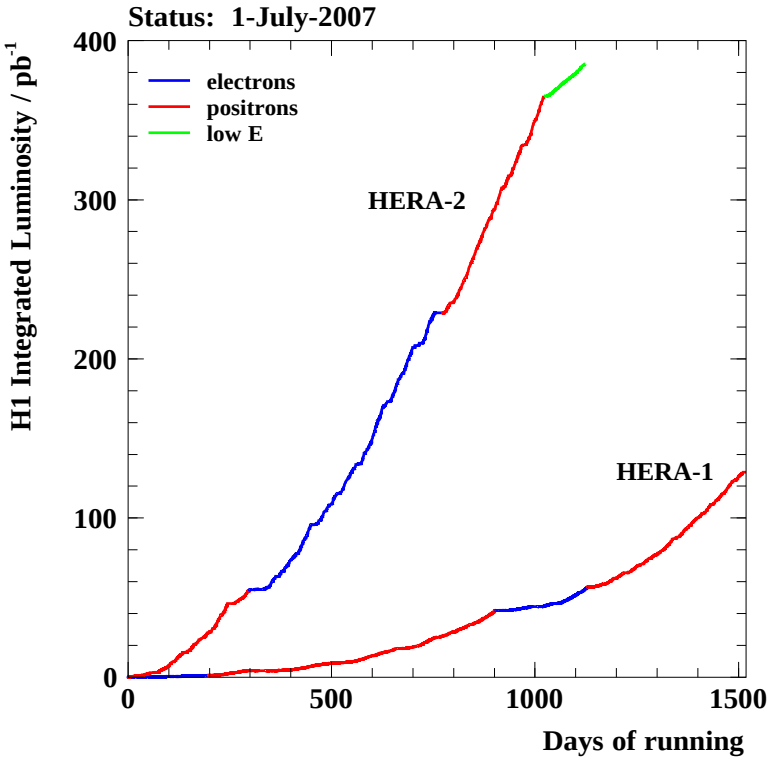

Introduction

HERA II

Through the emission of synchrotron radiation electron beam at HERA becomes transversely polarized

Spin Rotators installed
to obtain longitudinal polarization at IP

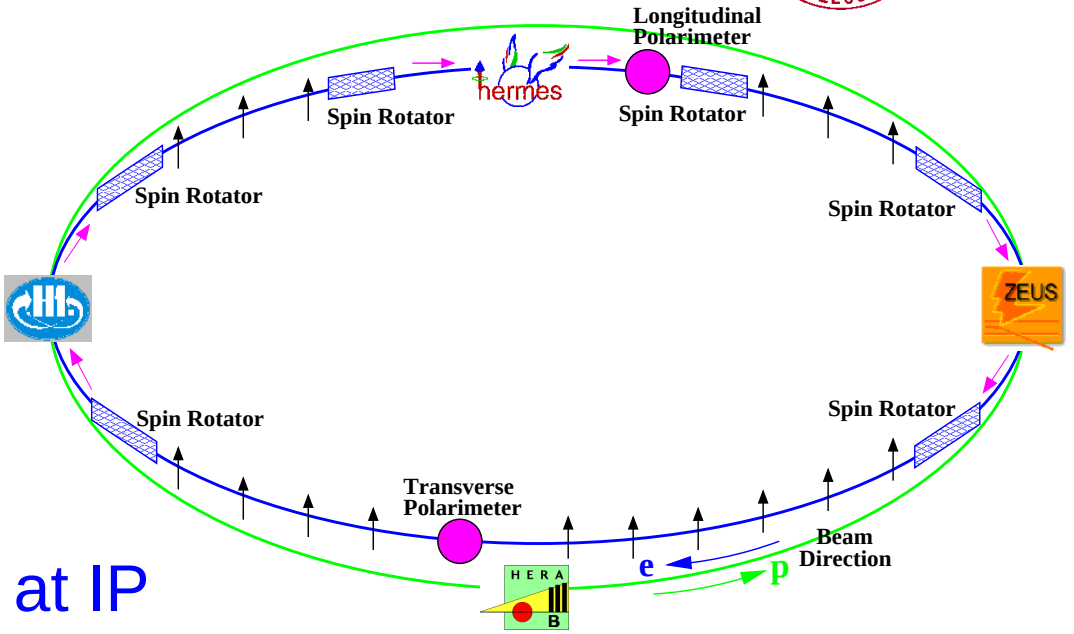

Introduction

HERA II

Through the emission of synchrotron radiation electron beam at HERA becomes transversely polarized

Spin Rotators installed
to obtain longitudinal polarization at IP

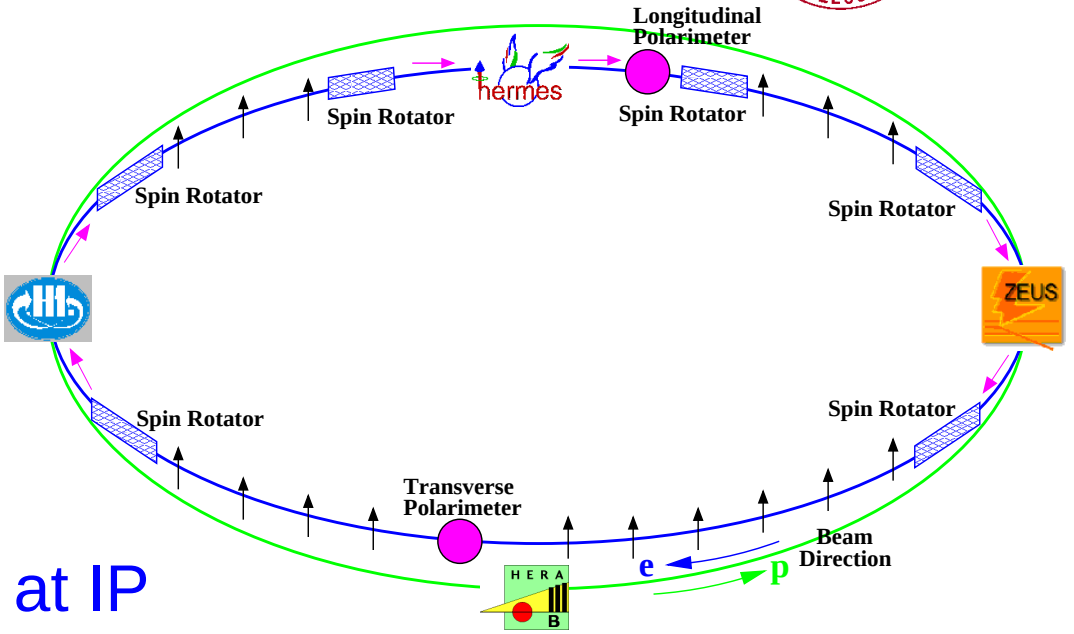

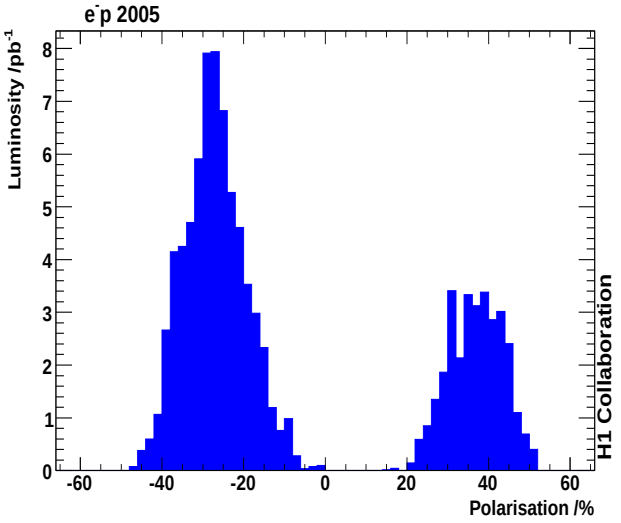

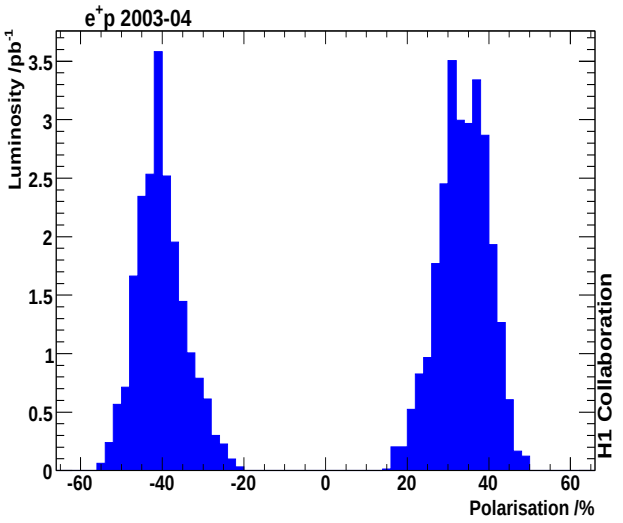

Polarization measured in dedicated polarimeters

Average polarization
30-40%

Introduction

H1

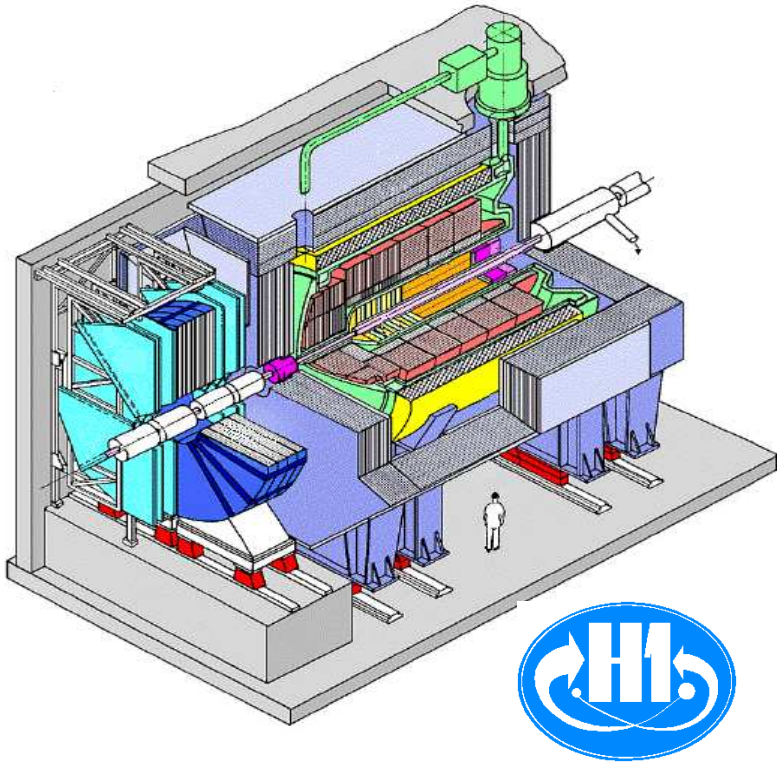

ZEUS

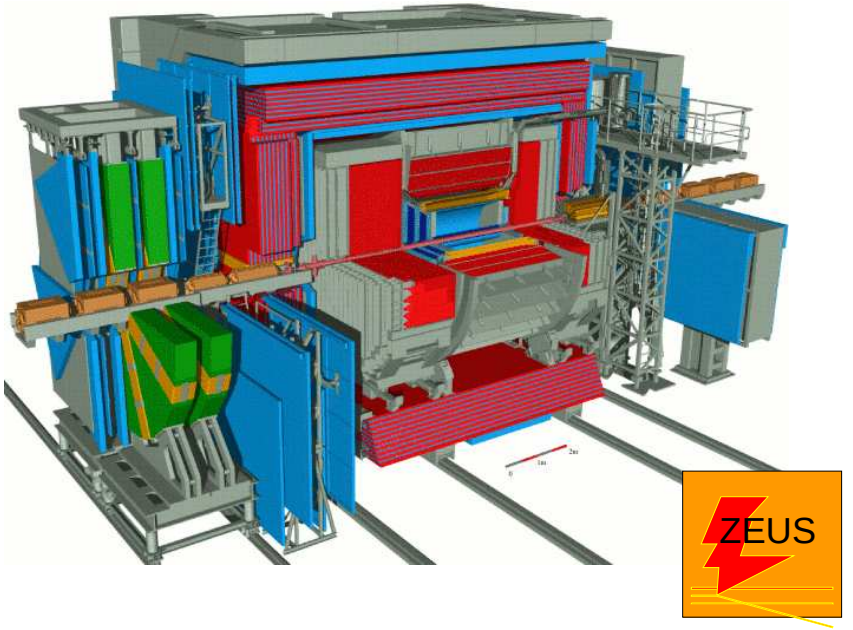

Two omni-purpose detectors

Both equipped with silicon tracking, drift chambers, hermetic calorimetry and muon detector system

Introduction

H1

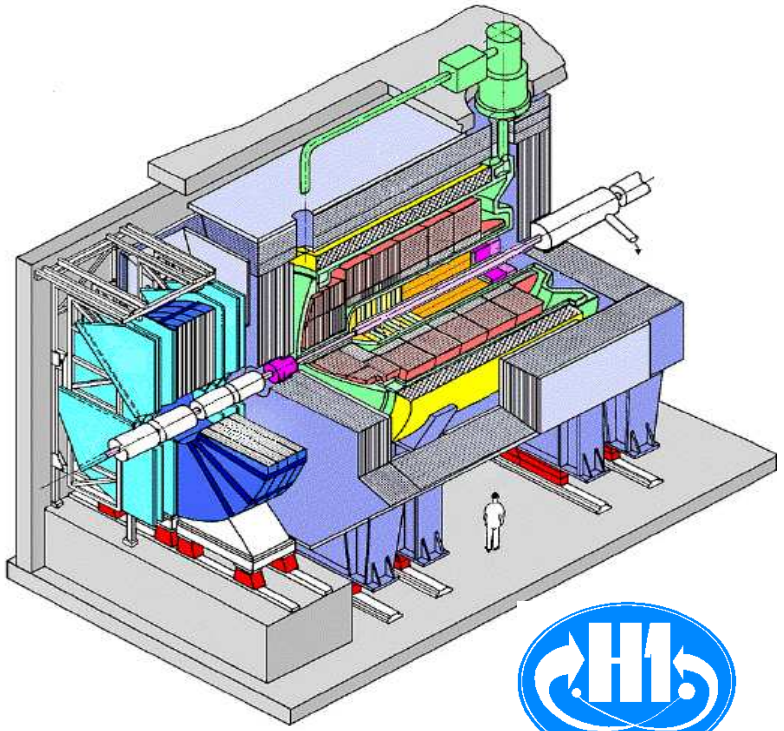

Fine-grained LAr calorimeter:

$$\sigma_E/E = 12\%/\sqrt{E} \oplus 1\% \quad \text{(ele)}$$

$$\sigma_E/E = 55\%/\sqrt{E} \oplus 1\% \quad \text{(had)}$$

Backward lead-scintillator calorimeter:

$$\sigma_E/E = 7\%/\sqrt{E} \oplus 1\% \quad \text{(ele)}$$

ZEUS

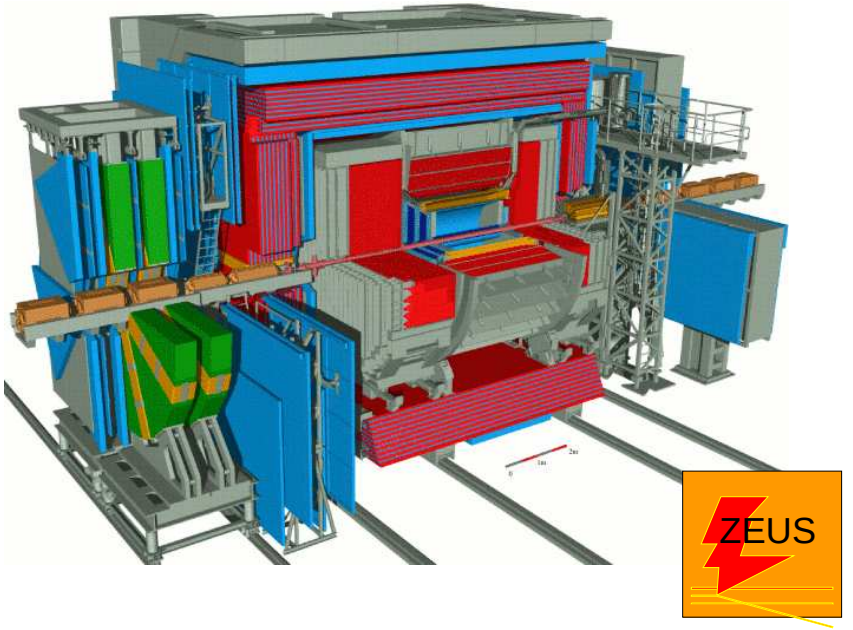

Uranium-scintillator calorimeter:

$$\sigma_E/E = 18\%/\sqrt{E} \quad \text{(ele)}$$

$$\sigma_E/E = 35\%/\sqrt{E} \quad \text{(had)}$$

Introduction

H1

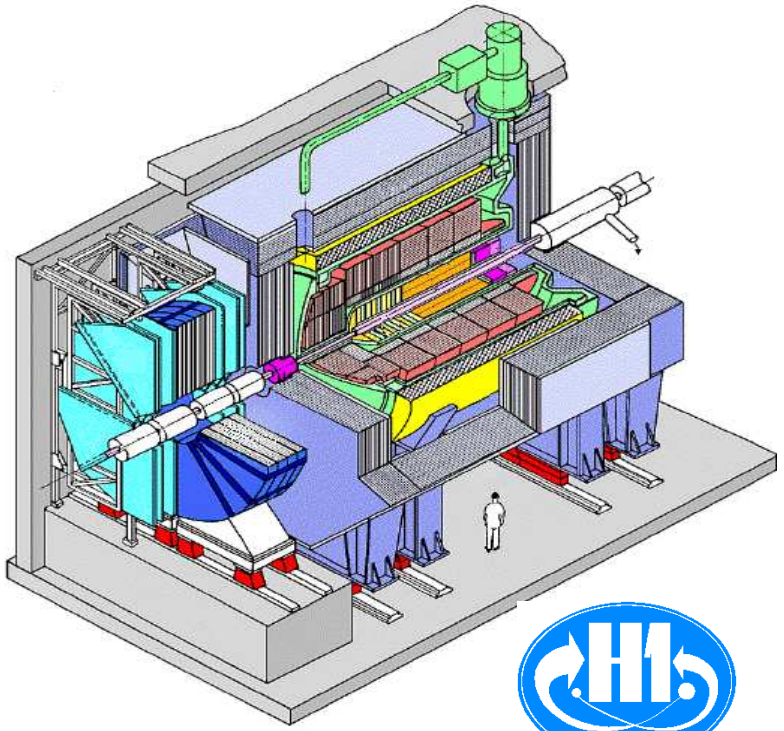

ZEUS

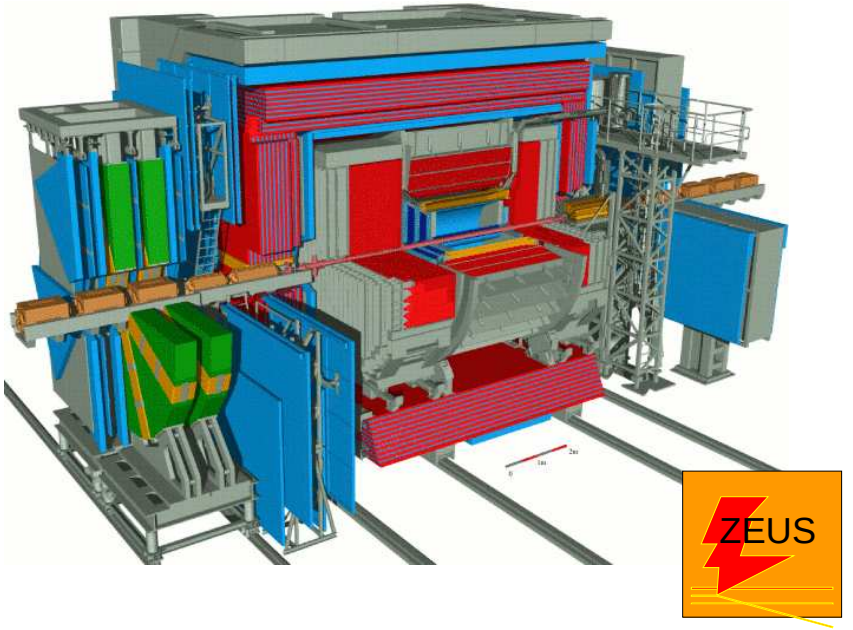

Combining H1 and ZEUS measurements

Different detectors

$\Rightarrow$ complementary event reconstruction methods

$\Rightarrow$ reduction of systematic uncertainties

Deep Inelastic $e^{\pm}p$ Scattering

Main process studied at H1 and ZEUS

NC DIS

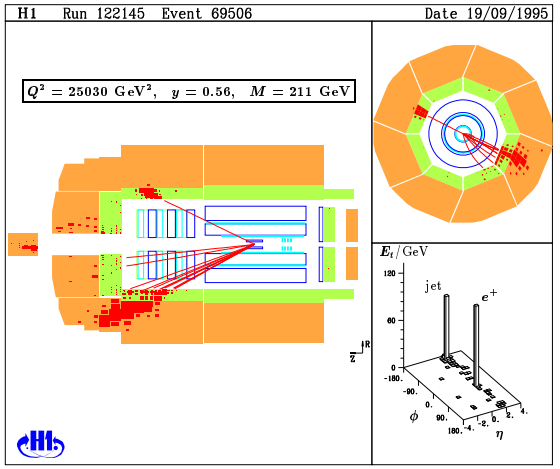

CC DIS

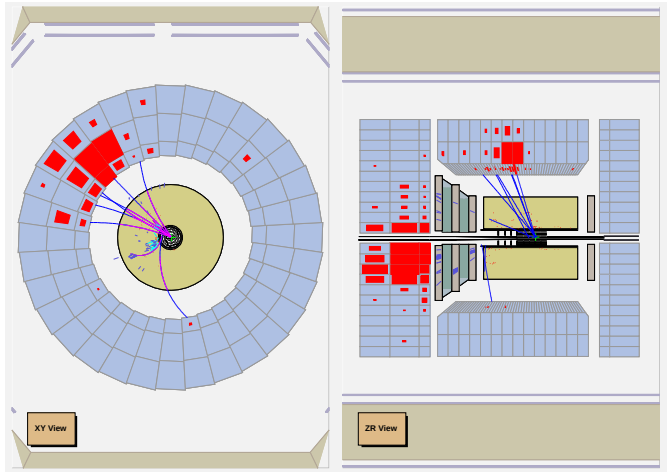

Kinematic variables:

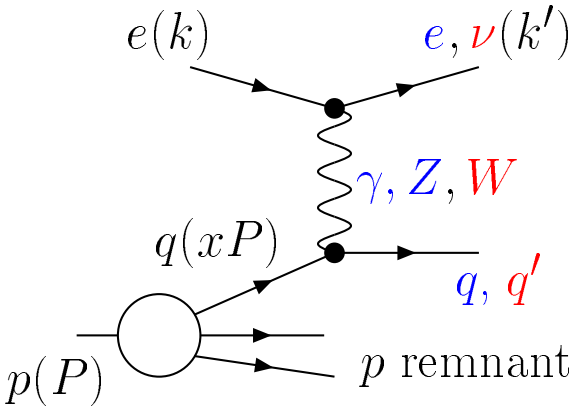

$$Q^2 = -(k - k')^2$$

$$x = \frac{Q^2}{2P \cdot (k - k')}$$

$$y = \frac{P \cdot (k - k')}{P \cdot k}$$

|virtuality| of the exchanged boson

$\Rightarrow$ spatial resolution $\lambda \sim 1/Q$

$\Rightarrow$ sensitivity to mass scales $\Lambda \sim Q$

Deep Inelastic $e^{\pm}p$ Scattering

Main process studied at H1 and ZEUS

NC DIS

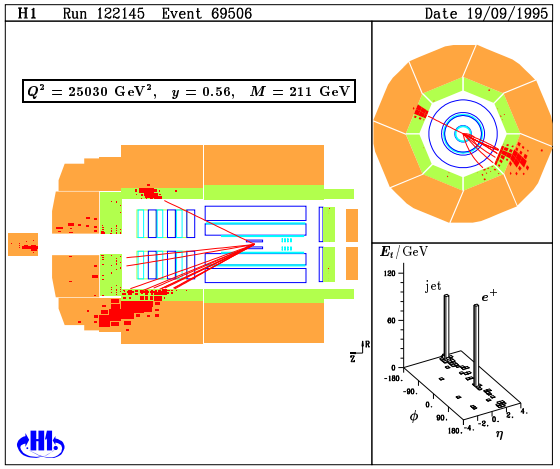

CC DIS

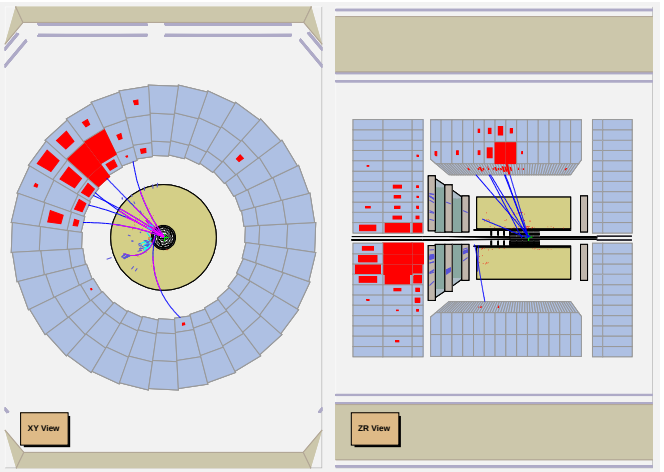

Kinematic variables:

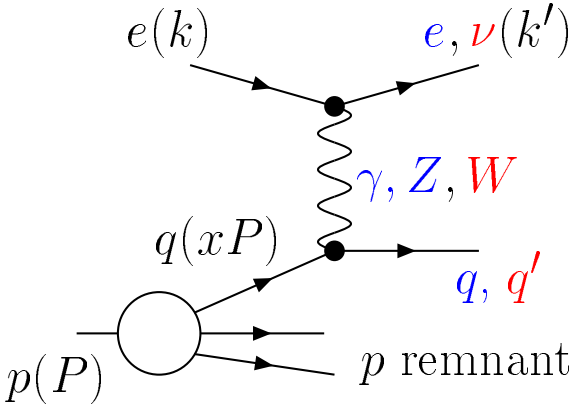

$$Q^2 = -(k - k')^2$$

|virtuality| of the exchanged boson

$$x = \frac{Q^2}{2P \cdot (k - k')}$$

fraction of proton momenta carried by stuck quark

$$y = \frac{P \cdot (k - k')}{P \cdot k}$$

fraction of lepton energy transfered in the proton rest frame

Deep Inelastic $e^{\pm}p$ Scattering

High-Q^2 NC & CC DIS

NC & CC comparable in size for

$$Q^2 \sim M_Z^2,\ M_W^2$$

Electroweak "unification"

Precise HERA data in excellent agreement with Standard Model predictions over many orders of magnitude.

$\Rightarrow$ test ground for SM and QCD

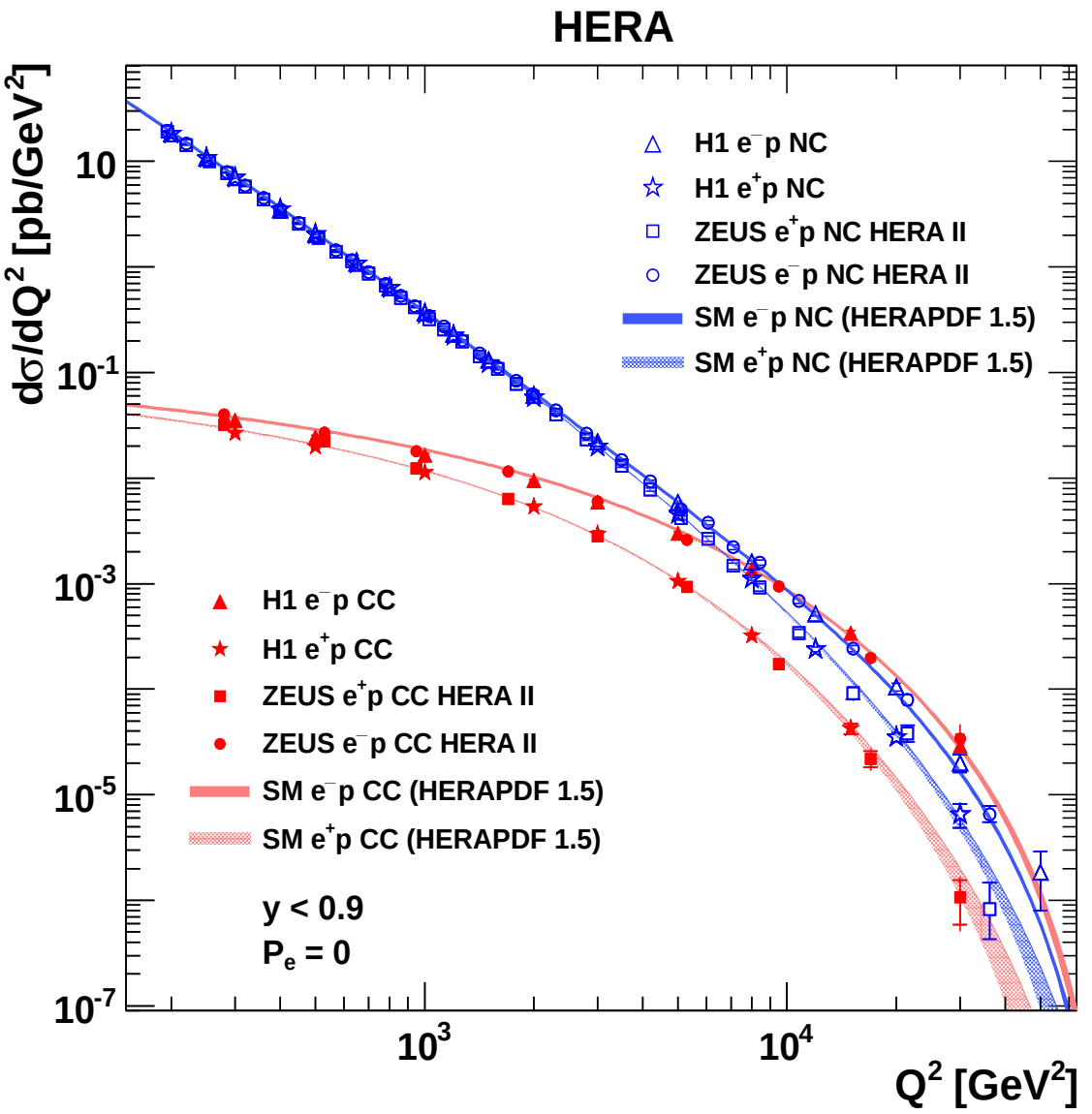

Deep Inelastic $e^{\pm}p$ Scattering

High Q^2 NC DIS cross section: neglecting radiative corrections

$$\frac{d^2\sigma^{\rm NC}(e^{\pm}p)}{dxdQ^2} = \frac{2\pi\alpha^2}{xQ^4}\left[Y_+\tilde{F}_2^{\pm} \mp Y_- x\tilde{F}_3^{\pm} - y^2\tilde{F}_L^{\pm}\right]$$

where: $Y_{\pm} = 1 \pm (1-y)^2$

Generalized structure functions: P_e - lepton beam polarization

$$\tilde{F}_2^{\pm} = F_2^{\gamma} - (v_e \pm P_e a_e)\chi_Z\, F_2^{\gamma Z} + (v_e^2 + a_e^2 \pm 2P_e v_e a_e)\chi_Z^2\, F_2^Z$$

$$x\tilde{F}_3^{\pm} = -(a_e \pm P_e v_e)\chi_Z\, xF_3^{\gamma Z} + (2v_e a_e \pm P_e(v_e^2 + a_e^2))\chi_Z^2\, xF_3^Z$$

$$\chi_Z = \frac{1}{\sin^2 2\theta_W}\left(\frac{Q^2}{M_Z^2 + Q^2}\right)$$

Deep Inelastic $e^{\pm}p$ Scattering

High Q^2 NC DIS cross section: neglecting radiative corrections

$$\frac{d^2\sigma^{\rm NC}(e^{\pm}p)}{dxdQ^2} = \frac{2\pi\alpha^2}{xQ^4}\left[Y_+\tilde{F}_2^{\pm} \mp Y_- x\tilde{F}_3^{\pm} - y^2\tilde{F}_L^{\pm}\right]$$

where: $Y_{\pm} = 1 \pm (1-y)^2$

Generalized structure functions: P_e - lepton beam polarization

$$\tilde{F}_2^{\pm} = F_2^{\gamma} - (v_e \pm P_e a_e)\chi_Z\, F_2^{\gamma Z} + (v_e^2 + a_e^2 \pm 2P_e v_e a_e)\chi_Z^2\, F_2^Z$$

$$x\tilde{F}_3^{\pm} = -(a_e \pm P_e v_e)\chi_Z\, xF_3^{\gamma Z} + (2v_e a_e \pm P_e(v_e^2 + a_e^2))\chi_Z^2\, xF_3^Z$$

$$\chi_Z = \frac{1}{\sin^2 2\theta_W}\left(\frac{Q^2}{M_Z^2 + Q^2}\right)$$

$\Rightarrow$ Polarization asymmetry sensitive to $F_2^{\gamma Z}$

Deep Inelastic $e^{\pm}p$ Scattering

High Q^2 NC DIS cross section: neglecting radiative corrections

$$\frac{d^2\sigma^{\rm NC}(e^{\pm}p)}{dxdQ^2} = \frac{2\pi\alpha^2}{xQ^4}\left[Y_+\tilde{F}_2^{\pm} \mp Y_- x\tilde{F}_3^{\pm} - y^2\tilde{F}_L^{\pm}\right]$$

where: $Y_{\pm} = 1 \pm (1-y)^2$

Generalized structure functions: P_e - lepton beam polarization

$$\tilde{F}_2^{\pm} = F_2^{\gamma} - (v_e \pm P_e a_e)\chi_Z\, F_2^{\gamma Z} + (v_e^2 + a_e^2 \pm 2P_e v_e a_e)\chi_Z^2\, F_2^Z$$

$$x\tilde{F}_3^{\pm} = -(a_e \pm P_e v_e)\chi_Z\, xF_3^{\gamma Z} + (2v_e a_e \pm P_e(v_e^2 + a_e^2))\chi_Z^2\, xF_3^Z$$

$$\chi_Z = \frac{1}{\sin^2 2\theta_W}\left(\frac{Q^2}{M_Z^2 + Q^2}\right)$$

$\Rightarrow$ Polarization asymmetry sensitive to $F_2^{\gamma Z}$

$\Rightarrow$ Charge asymmetry used to extract $xF_3^{\gamma Z}$

Deep Inelastic $e^{\pm}p$ Scattering

High Q^2 NC DIS cross section: neglecting radiative corrections

$$\frac{d^2\sigma^{\rm NC}(e^{\pm}p)}{dxdQ^2} = \frac{2\pi\alpha^2}{xQ^4}\left[Y_+\tilde{F}_2^{\pm} \mp Y_- x\tilde{F}_3^{\pm} - y^2\tilde{F}_L^{\pm}\right]$$

where: $Y_{\pm} = 1 \pm (1-y)^2$

Generalized structure functions: P_e - lepton beam polarization

$$\tilde{F}_2{}^{\pm} = \sum_q x(q+\bar{q})\left[e_q^2 - 2e_q v_q (v_e \pm P_e a_e)\chi Z + (v_q^2+a_q^2)(v_e^2+a_e^2 \pm 2P_e v_e a_e)\chi_Z^2\right]$$

$$x\tilde{F}_3{}^{\pm} = \sum_q 2x(q-\bar{q})\left[-e_q a_q (a_e \pm P_e v_e)\chi Z + v_q a_q (2v_e a_e \pm P_e(v_e^2+a_e^2))\chi_Z^2\right]$$

$$\chi_Z = \frac{1}{\sin^2 2\theta_W}\left(\frac{Q^2}{M_Z^2+Q^2}\right)$$

$\Rightarrow$ Polarization asymmetry sensitive to $F_2^{\gamma Z}$ $\Rightarrow$ vector quark couplings, v_q

$\Rightarrow$ Charge asymmetry used to extract $xF_3^{\gamma Z}$ $\Rightarrow$ axial quark couplings, a_q

Deep Inelastic $e^{\pm}p$ Scattering

Polarization asymmetries

Direct measurement of parity violation due to $\gamma - Z$ interference

$$A^{\pm} = \frac{2}{P_L^{\pm} - P_R^{\pm}} \cdot \frac{\sigma^{e^{\pm}p}(P_L^{\pm}) - \sigma^{e^{\pm}p}(P_R^{\pm})}{\sigma^{e^{\pm}p}(P_L^{\pm}) + \sigma^{e^{\pm}p}(P_R^{\pm})}$$

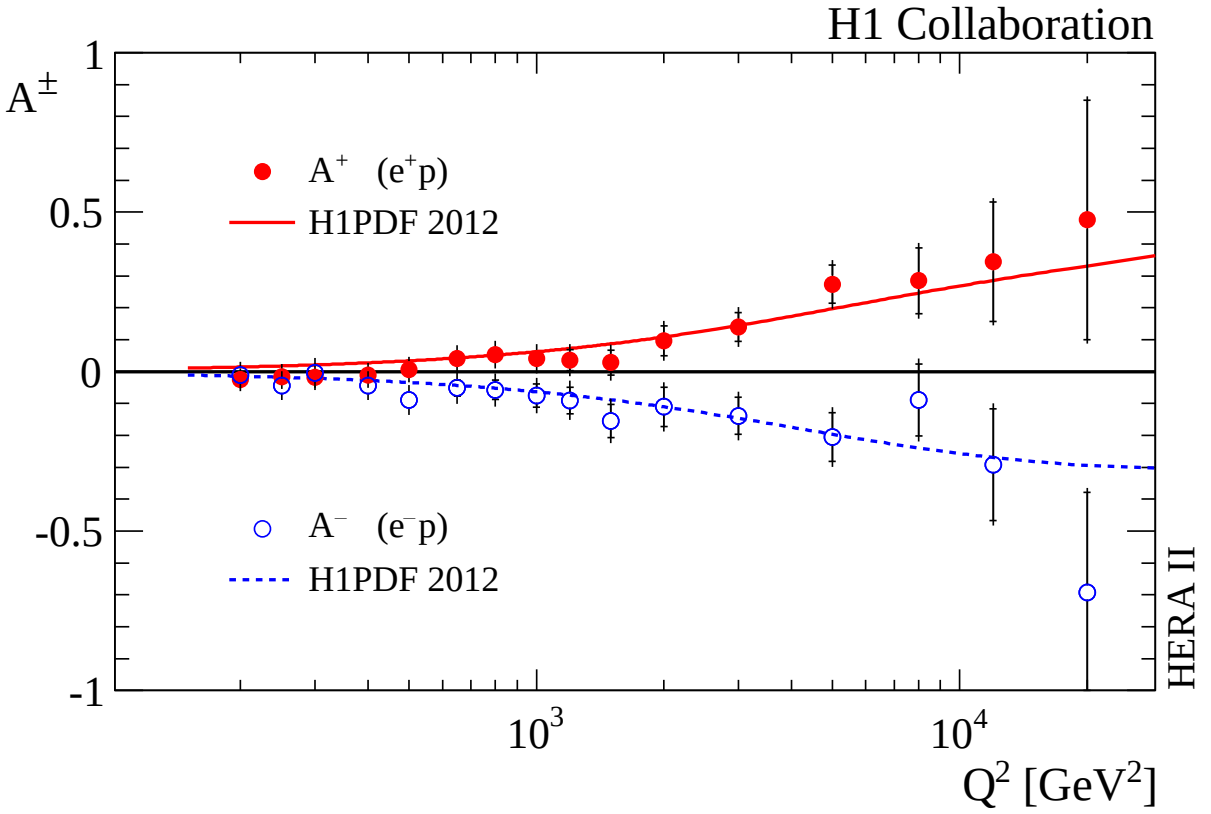

Deep Inelastic $e^{\pm}p$ Scattering

Polarization asymmetries

Direct measurement of parity violation due to $\gamma - Z$ interference

$$A^{\pm} = \frac{2}{P_L^{\pm} - P_R^{\pm}} \cdot \frac{\sigma^{e^{\pm}p}(P_L^{\pm}) - \sigma^{e^{\pm}p}(P_R^{\pm})}{\sigma^{e^{\pm}p}(P_L^{\pm}) + \sigma^{e^{\pm}p}(P_R^{\pm})} \approx \mp a_e \chi_Z \frac{F_2^{\gamma Z}}{\tilde{F}_2}$$

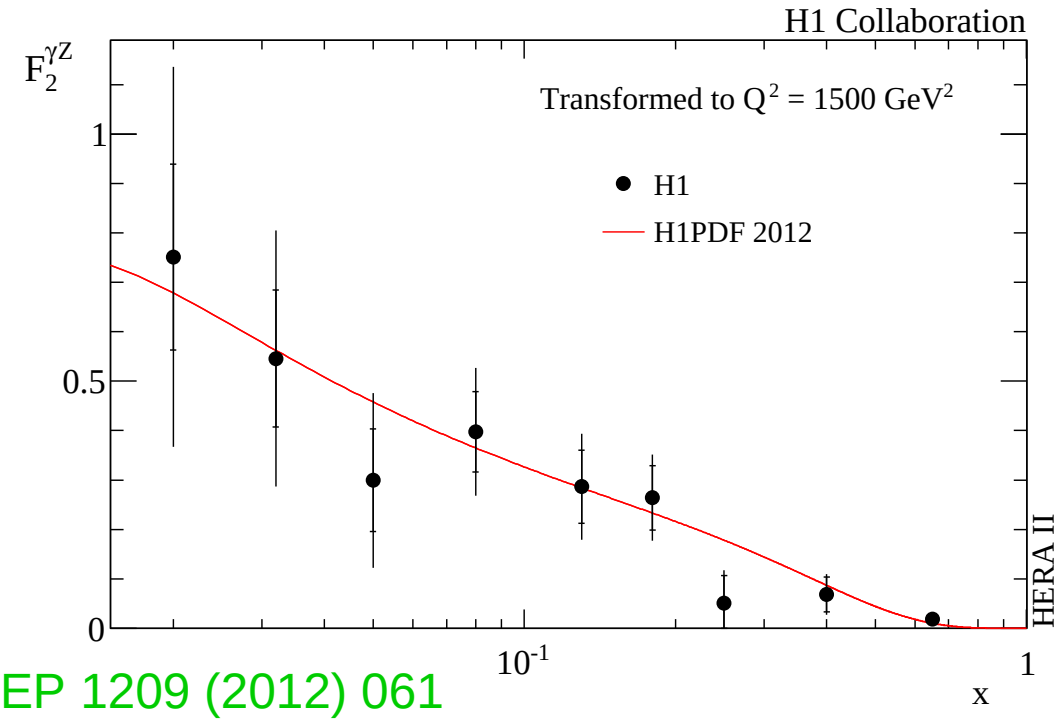

JHEP 1209 (2012) 061

$$F_2^{\gamma Z} = \sum_q 2x(q + \bar{q})\, e_q\, v_q$$

$$\sim u + \bar{u} + d + \bar{d}$$

At high-x:

$$A^{\pm} \sim \pm \frac{1 + d/u}{4 + d/u}$$

$\Rightarrow$ constrains d/u ratio

Deep Inelastic $e^{\pm}p$ Scattering

Charge asymmetry

Measurement of $xF_3^{\gamma Z}$ from combined e^+p and e^-p data.

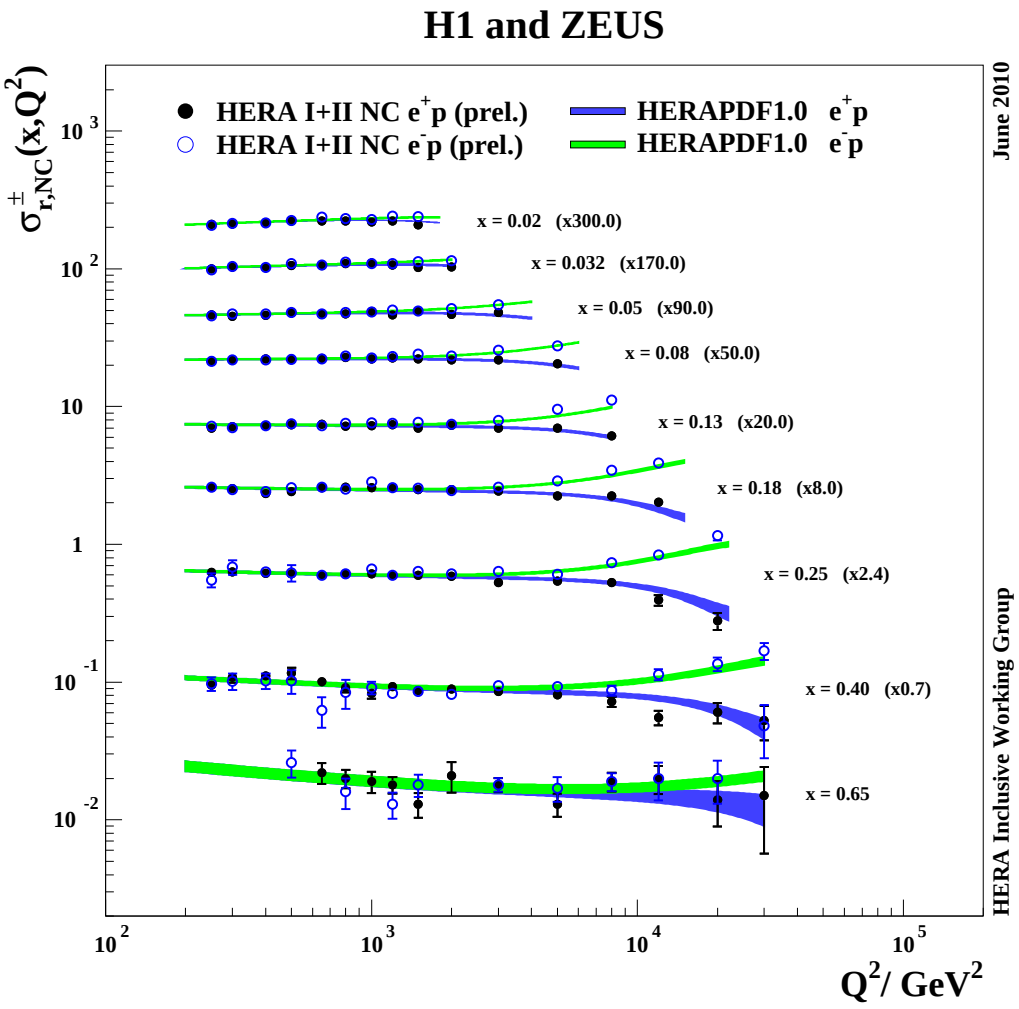

Deep Inelastic $e^{\pm}p$ Scattering

Charge asymmetry

Measurement of $xF_3^{\gamma Z}$ from combined e^+p and e^-p data.

Assuming SM couplings:

$$xF_3^{\gamma Z} \approx \left(\frac{2}{3}u_v + \frac{1}{3}d_v\right)x$$

$\Rightarrow$ constrains valence quarks

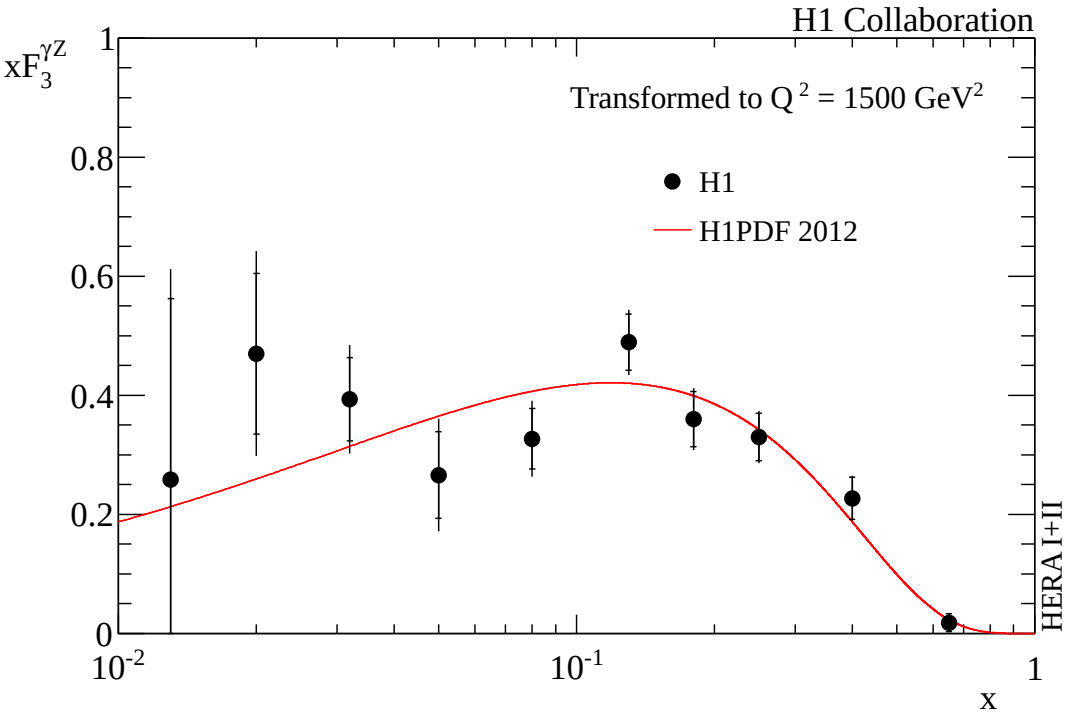

JHEP 1209 (2012) 061

Deep Inelastic $e^{\pm}p$ Scattering

Charge asymmetry

Measurement of $xF_3^{\gamma Z}$ from combined e^+p and e^-p data.

Assuming SM couplings:

$$xF_3^{\gamma Z} \approx \left(\frac{2}{3}u_v + \frac{1}{3}d_v\right)x$$

$\Rightarrow$ constrains valence quarks

Well described by different PDF sets

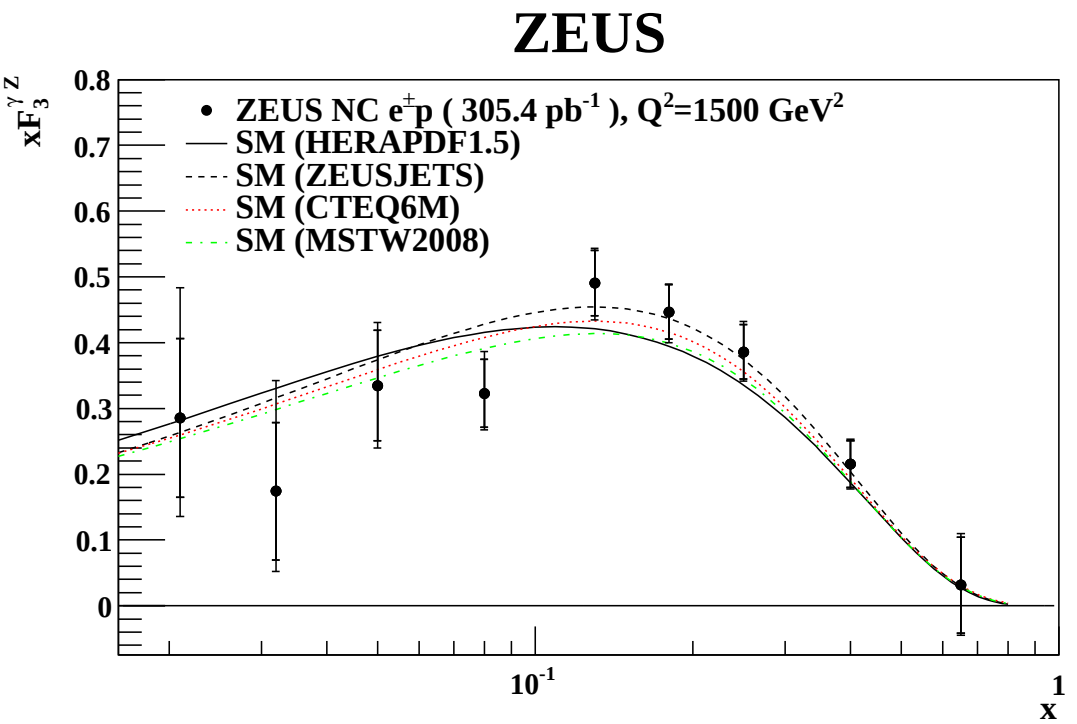

submitted to EPJ C

Deep Inelastic $e^{\pm}p$ Scattering

CC DIS Cross section

Polarization dependence:

$$\frac{d^2\sigma^{e^{\pm}p}}{dxdQ^2} = (1 \pm P_e)\frac{G_F^2}{4\pi x}\left(\frac{M_W^2}{M_W^2+Q^2}\right)^2 \times \begin{cases} x\left[u+c+(1-y)^2(\bar{d}+\bar{s}+\bar{b})\right] & for \quad e^-p \\ x\left[(1-y)^2(d+s+b)+\bar{u}+\bar{c}\right] & for \quad e^+p \end{cases}$$

constraints on u and d densities at high x

Measurements confirm chiral structure of SM

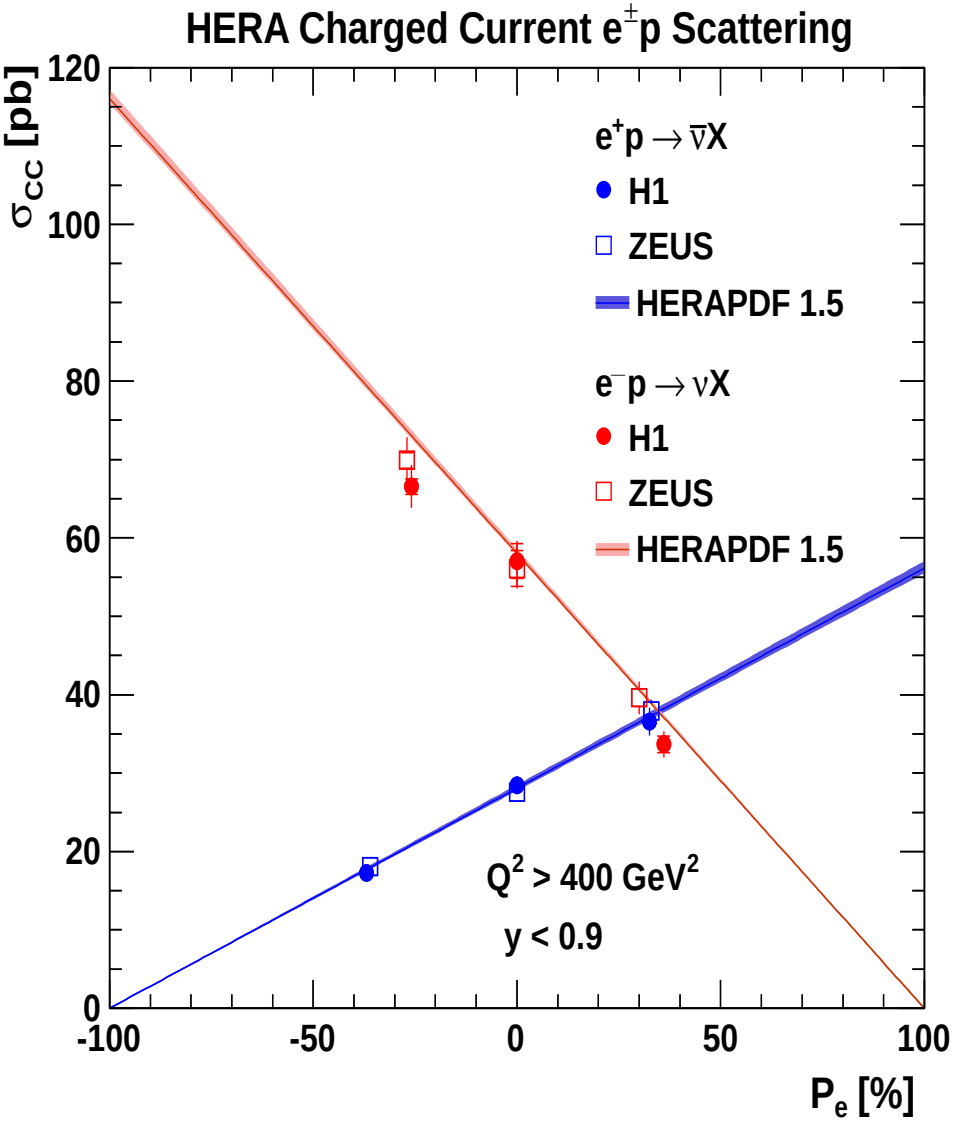

Deep Inelastic $e^{\pm}p$ Scattering

CC DIS Cross section

Polarization dependence:

$$\frac{d^2\sigma^{e^{\pm}p}}{dxdQ^2} = (1 \pm P_e)\frac{G_F^2}{4\pi x}\left(\frac{M_W^2}{M_W^2+Q^2}\right)^2 \times \begin{cases} x\left[u+c+(1-y)^2(\bar{d}+\bar{s}+\bar{b})\right] & for \quad e^-p \\ x\left[(1-y)^2(d+s+b)+\bar{u}+\bar{c}\right] & for \quad e^+p \end{cases}$$

constraints on u and d densities at high x

H1 excludes right handed charged currents for

$$M_W^R < 214GeV \quad e^-p$$
$$< 194GeV \quad e^+p$$

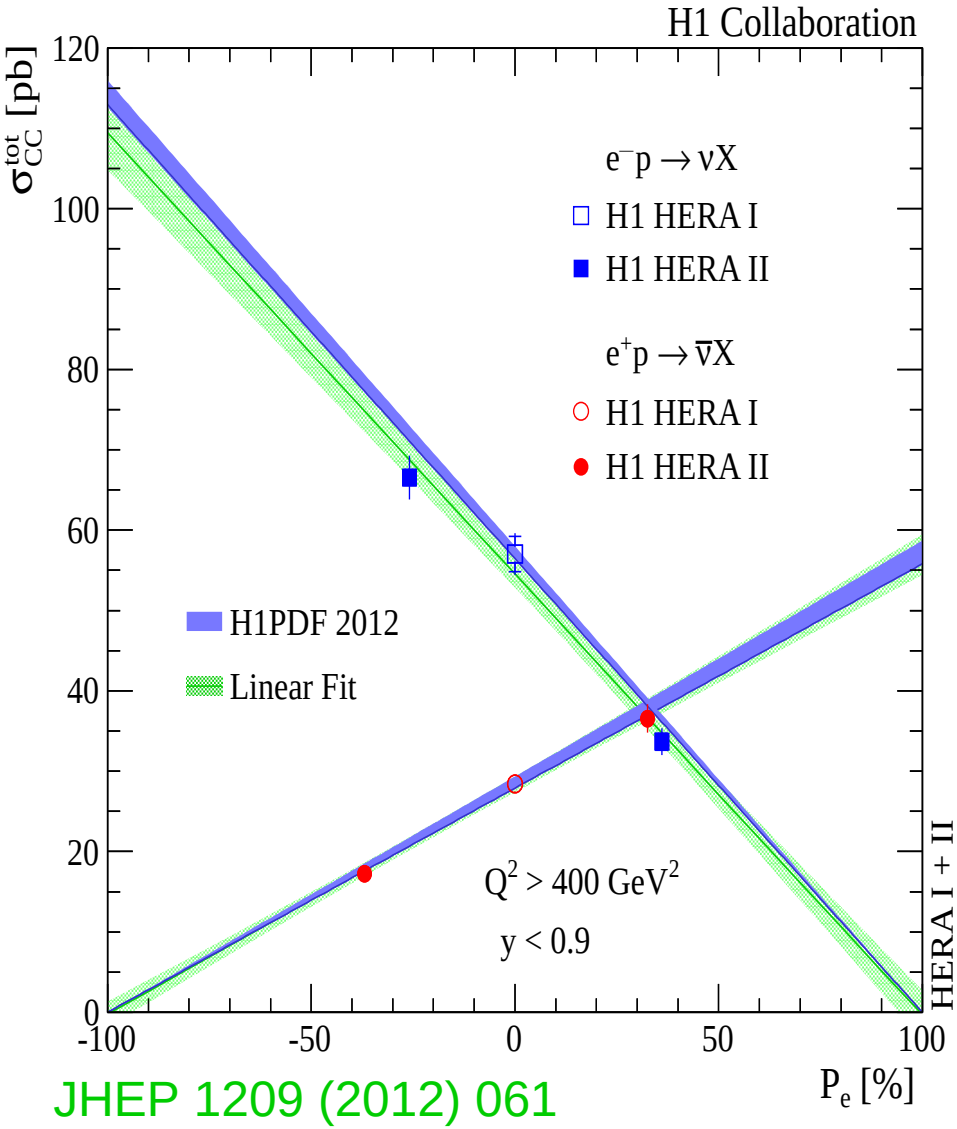

JHEP 1209 (2012) 061

Deep Inelastic $e^{\pm}p$ Scattering

Combined QCD and Electroweak analysis

High precision of NC and CC DIS measurements for polarized $e^{-}p$ and $e^{+}p$ allow for simultaneous determination of PDFs and electroweak parameters:

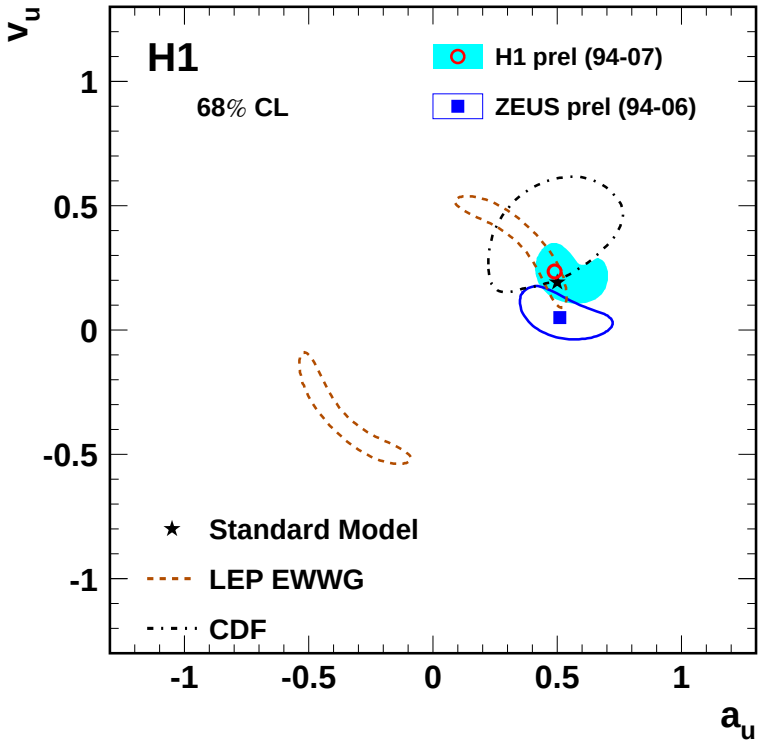

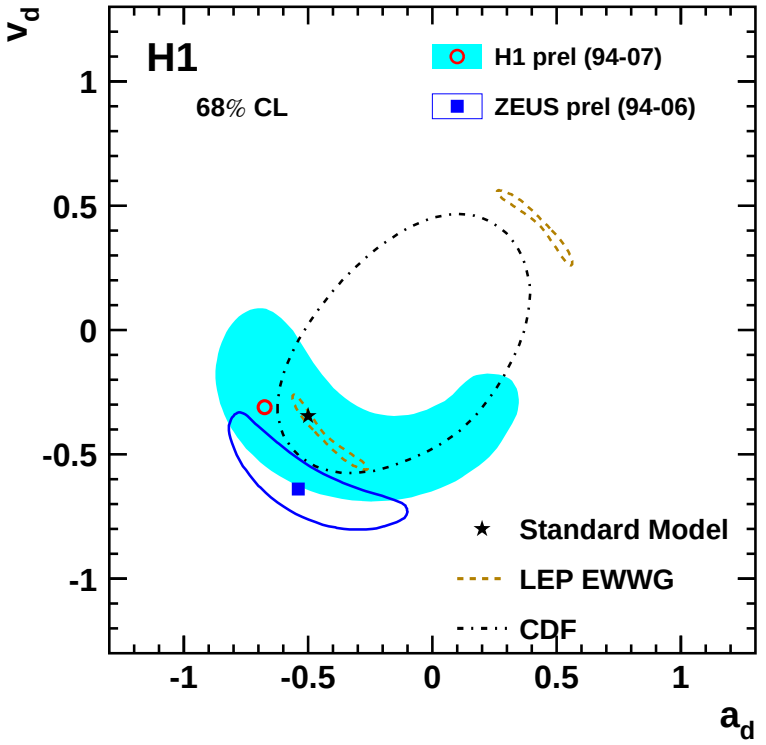

$\Rightarrow$ Precision of light quark EW coupling determination similar to Tevatron and LEP.
No sign ambiguity.

H1prelim-10-042

Deep Inelastic $e^{\pm}p$ Scattering

Contact Interactions

HERA data in perfect agreement with SM predictions

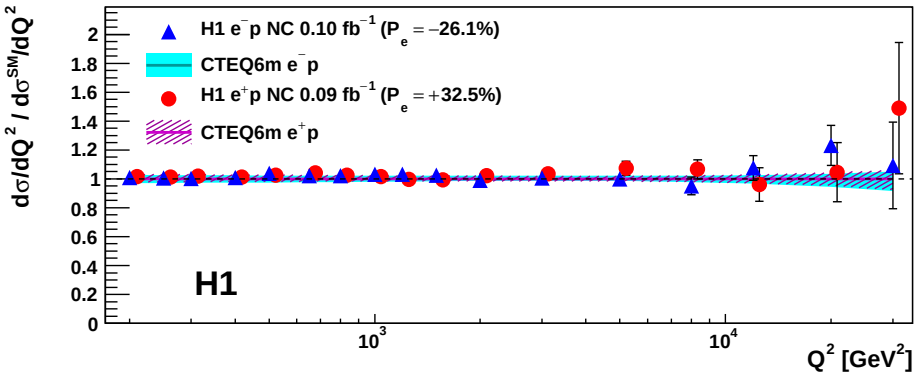

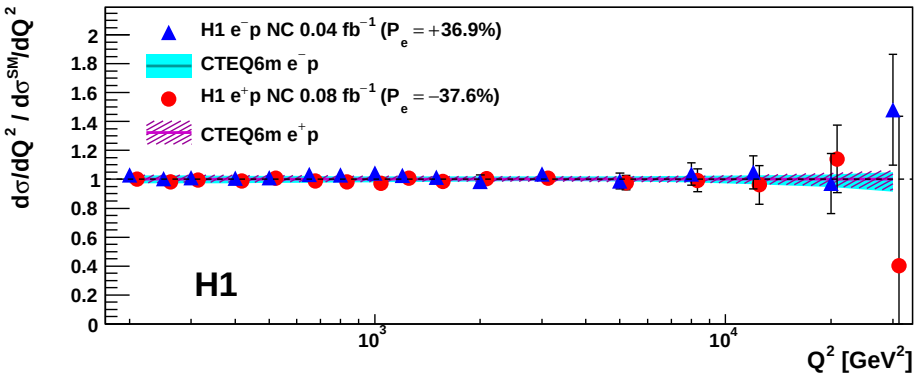

Assuming that $\sqrt{s}$ is much smaller than "new physics" scale Λ

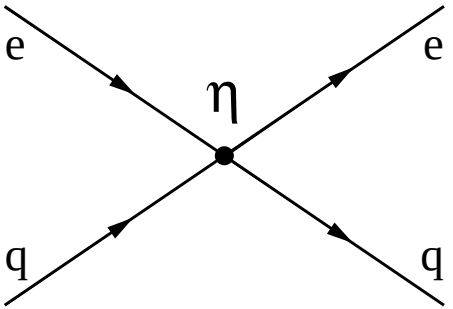

$eeqq$ contact interactions (CI)

Effective Lagrangian for vector $eeqq$ contact interactions:

$$\mathcal{L}_{CI} = \sum_{\substack{\alpha,\beta=L,R \\ q}} \eta^{eq}_{\alpha\beta} \cdot (\bar{e}_\alpha \gamma^\mu e_\alpha)(\bar{q}_\beta \gamma_\mu q_\beta)$$

$\eta^{eq}_{\alpha\beta}$ - 4 possible couplings for every flavor

Deep Inelastic $e^{\pm}p$ Scattering

Contact Interactions

HERA data in perfect agreement with SM predictions

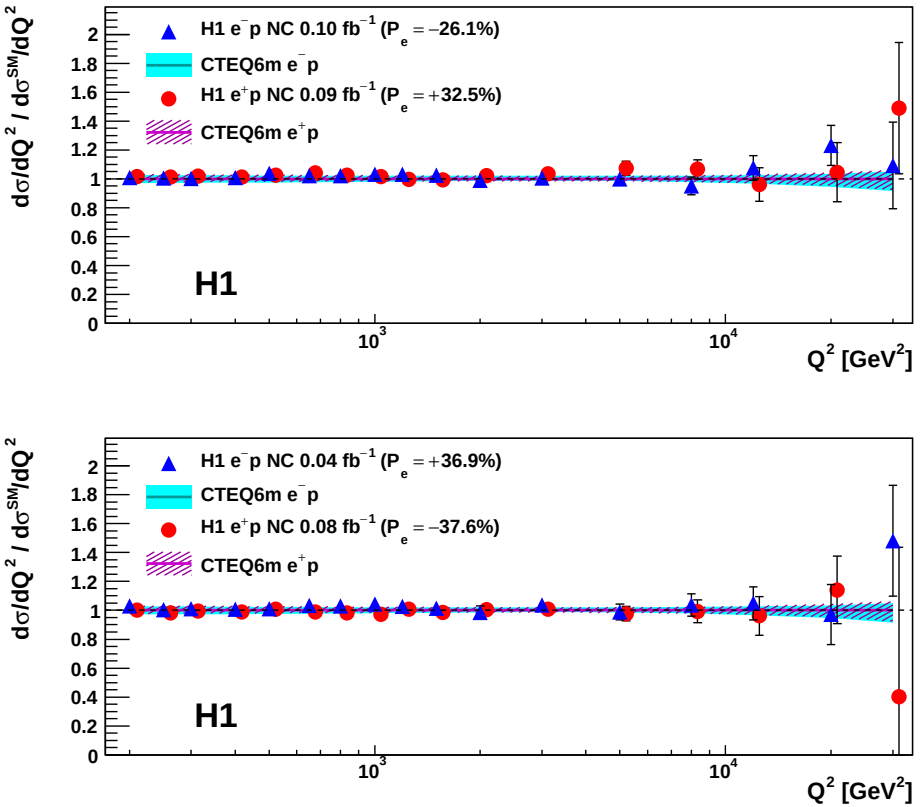

H1 limits on compositeness scale in general CI model:

$\Lambda > 3.6$ - 7.2 TeV (95% C.L.)

depending on the chiral structure

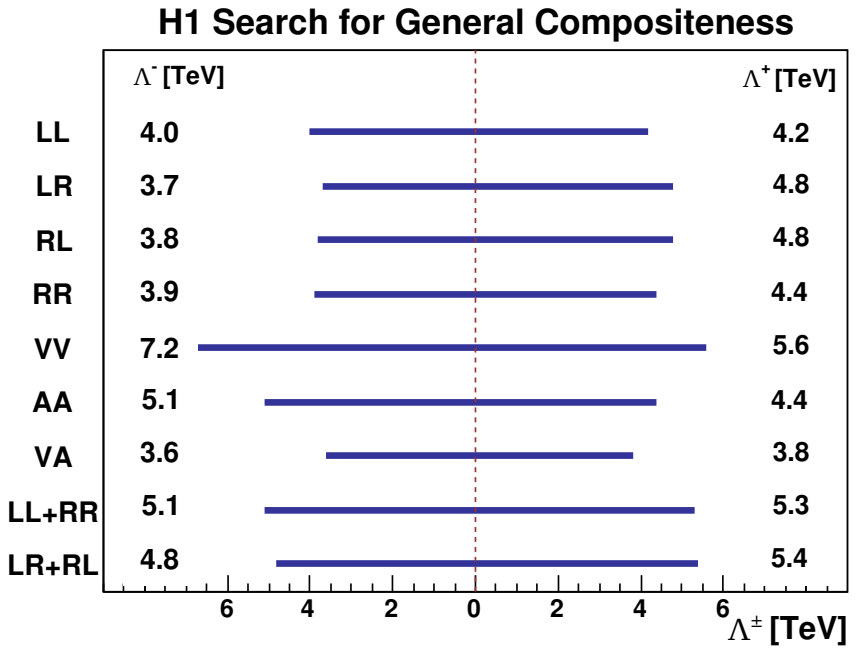

Deep Inelastic $e^{\pm}p$ Scattering

Contact Interactions

HERA data in perfect agreement with SM predictions

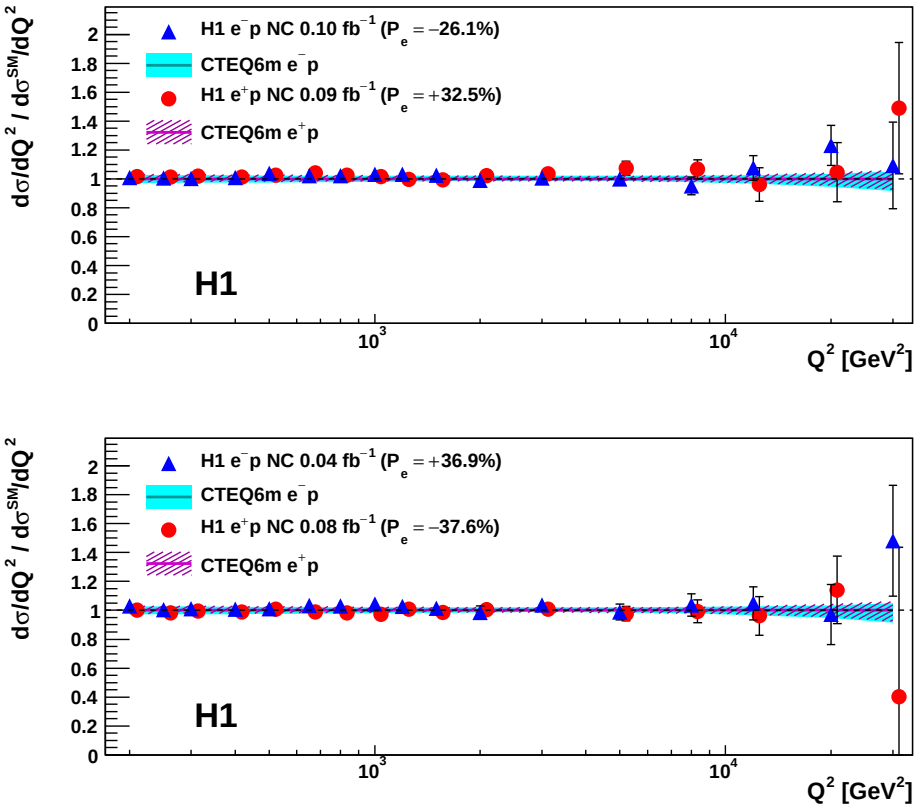

H1 limits on compositeness scale in general CI model:

$\Lambda > 3.6$ - 7.2 TeV (95% C.L.)

depending on the chiral structure

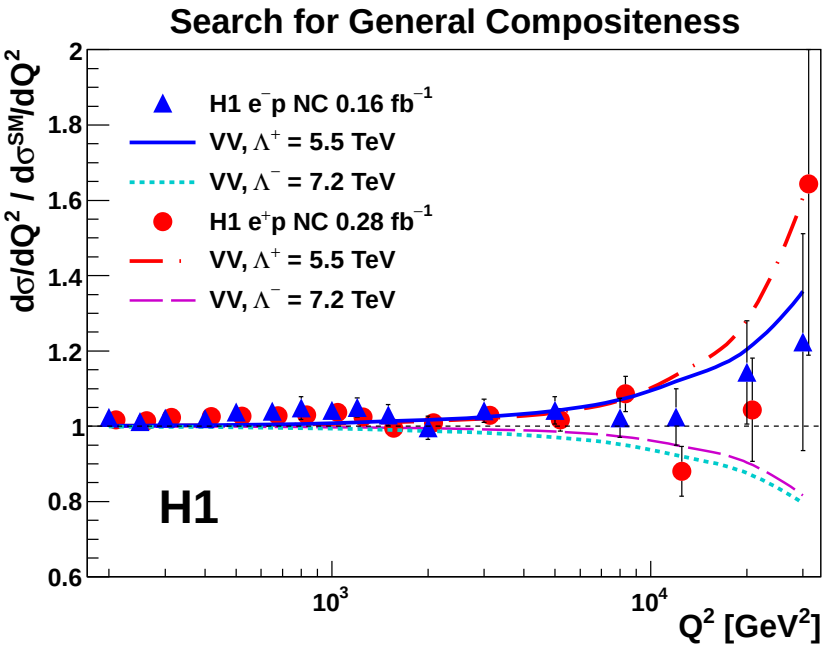

Deep Inelastic $e^{\pm}p$ Scattering

Contact Interactions

HERA data in perfect agreement with SM predictions

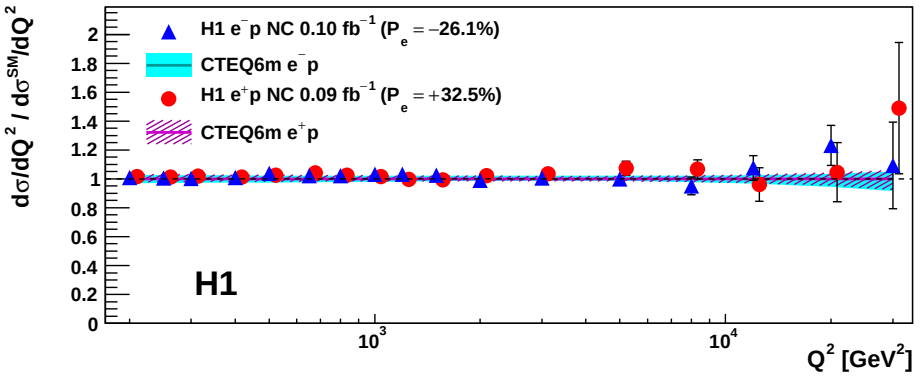

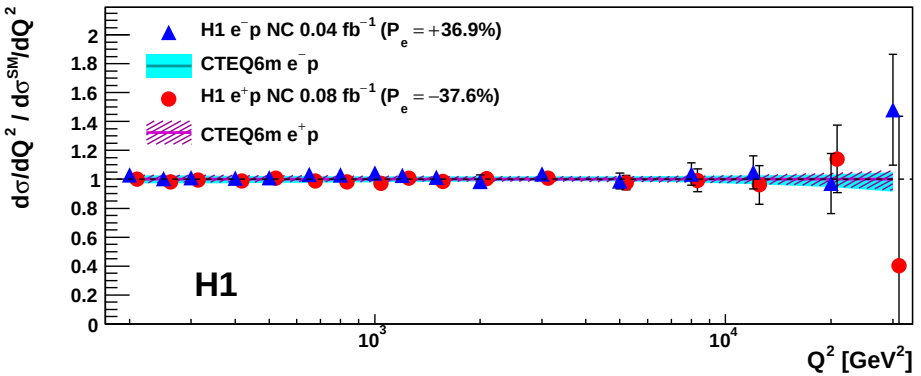

H1 limits on compositeness scale in general CI model:

$\Lambda > 3.6$ - 7.2 TeV (95% C.L.)

depending on the chiral structure

Leptoquark limits:

$M_{LQ}/\lambda > 0.41$ - 1.86 TeV

Large Extra Dimensions:

$M_S > 0.9$ TeV

Quark radius:

$R_q < 0.65 \cdot 10^{-18}$ m

Phys.Lett. B705 (2011) 52-58

Electroweak cross sections

$W^{\pm}$ production

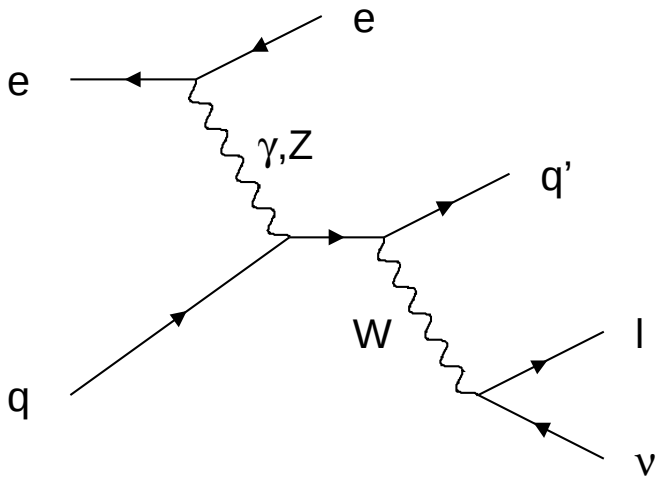

Signatures of single W boson production:

quark jet

isolated lepton $\Rightarrow$ large transverse momentum p_T^l

neutrino $\Rightarrow$ large missing transverse momentum p_T

Cross section measurement accessible only with the full HERA high energy data.

Combined H1 and ZEUS samples:

81 events observed, 87.8 ± 11.0 events expected.

Electroweak cross sections

$W^{\pm}$ production

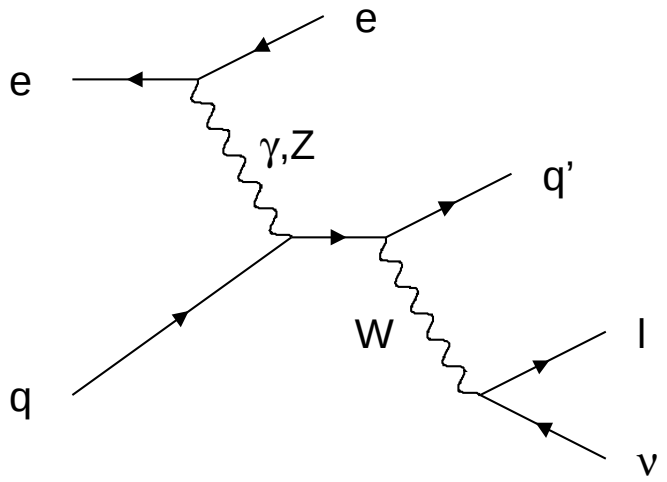

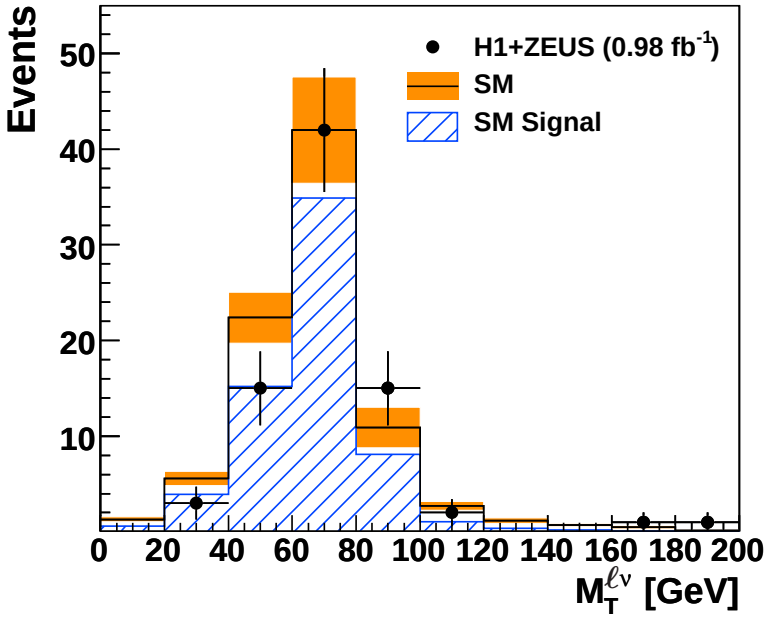

Inclusive single W production cross section (H1+ZEUS combined, $0.98\ fb^{-1}$):

$$\sigma_W \quad = \quad 1.06 \pm 0.16(stat.) \pm 0.07(sys.)\ pb$$

In agreement with the SM prediction: JHEP 3 (2010) 1-19

$$\sigma_W^{SM} \quad = \quad 1.26 \pm 0.19\ pb$$

Electroweak cross sections

Z° production

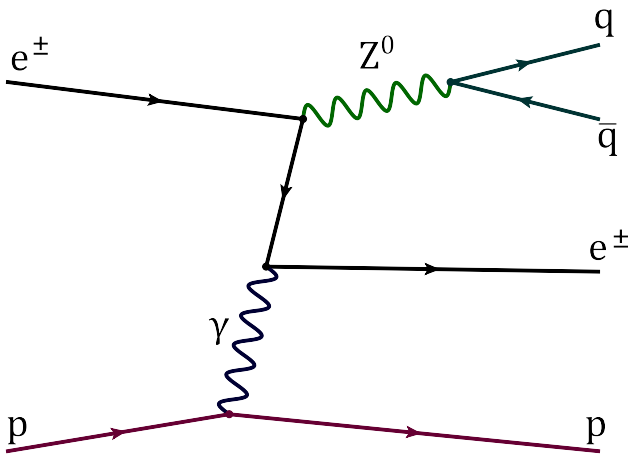

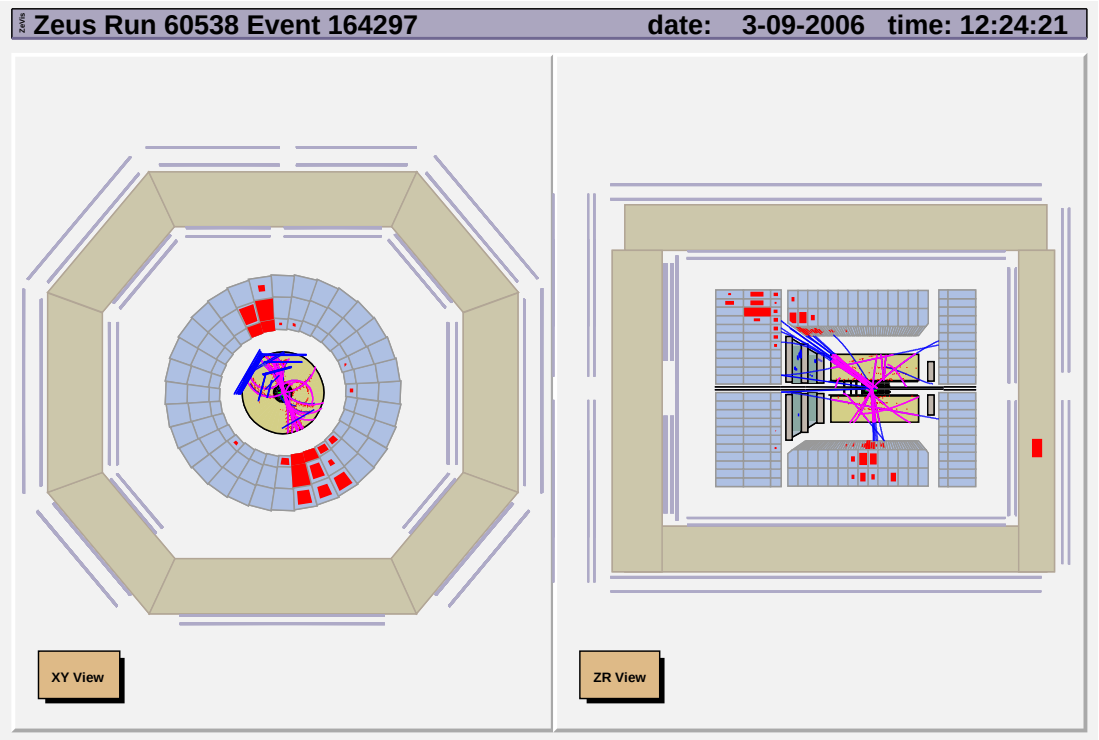

$$M_{jj} = 91.7\ GeV$$

Expected SM cross section $\sim 0.4\ pb$

$\Rightarrow$ only hadronic decays accessible (leptonic BR too small)

Electroweak cross sections

Z° production

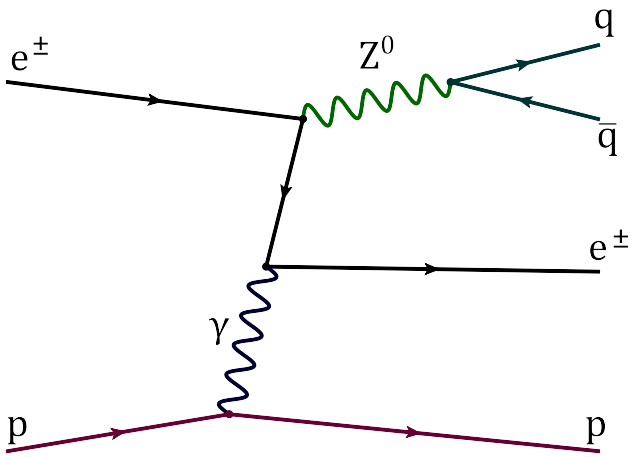

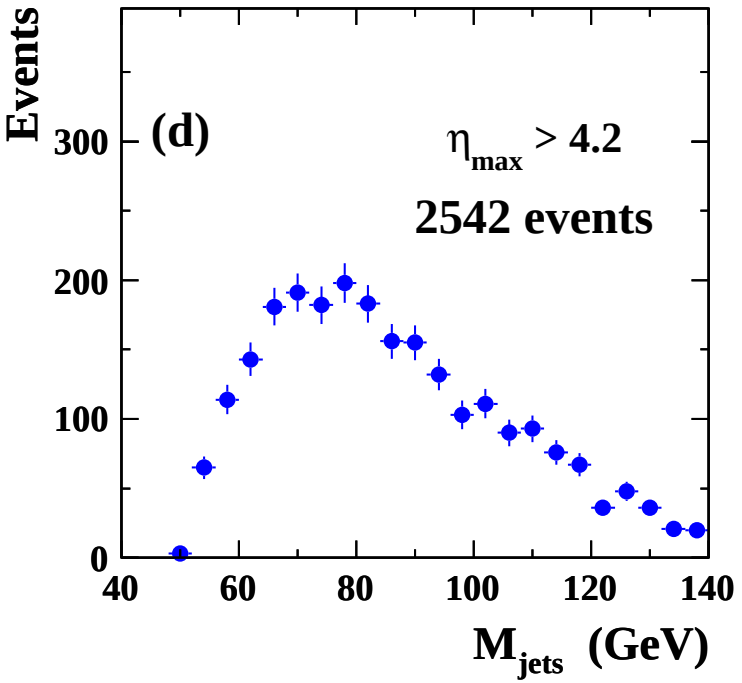

Hadronic Z° decays

$\Rightarrow$ very large QCD multi-jet background

Electroweak cross sections

Z° production

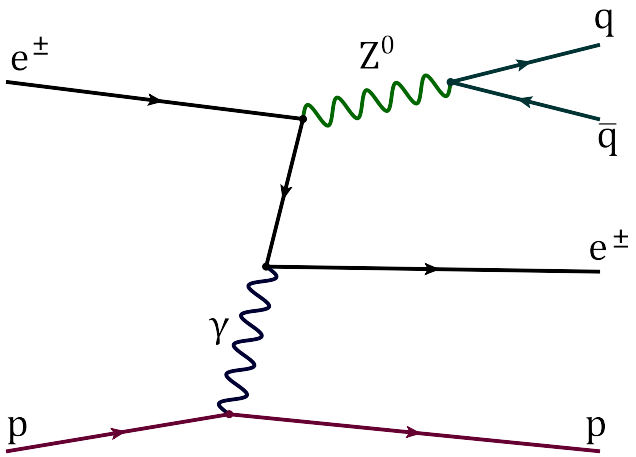

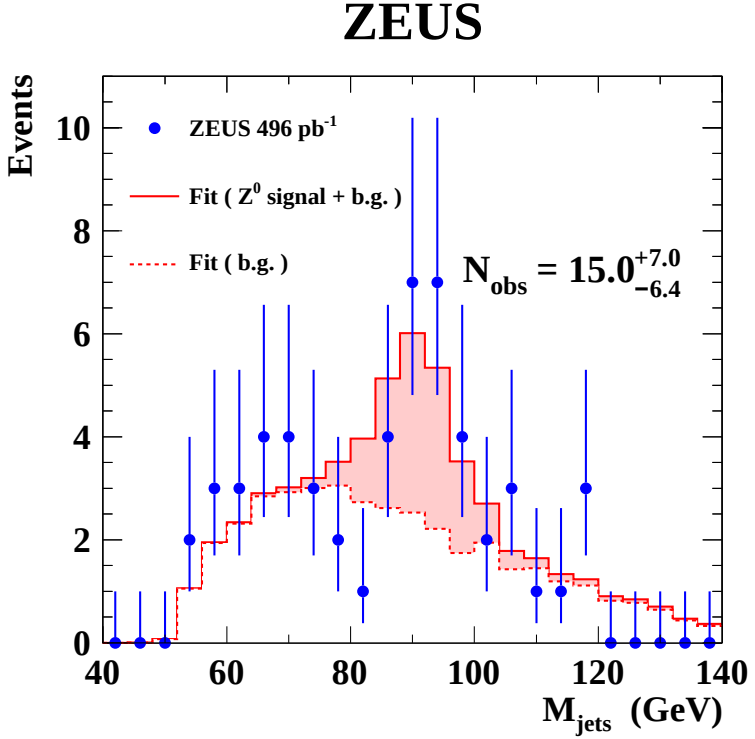

Better S/B ratio for elastic events, selected with a requirement $\eta_{max} < 3.0$

η_{max} - pseudorapidity of the most forward energy deposit in the calorimeter

$$\sigma(ep \to ep^{(*)} Z^\circ) = 0.13 \pm 0.06(stat.) \pm 0.01(syst.)\ pb$$

$$\sigma^{SM} = 0.16\ pb$$

Phys. Lett. B 718 (2013) 915-921

Electroweak cross sections

Single top production

SM cross section below 1 fb^{-1}

FCNC couplings can induce single-top production in several BSM extensions

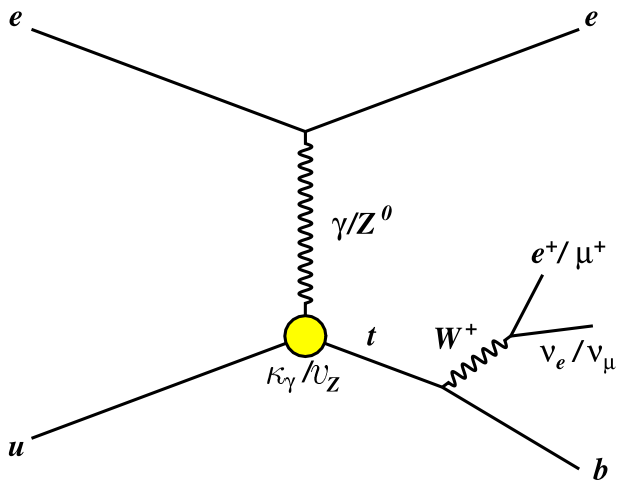

Signatures of $t \to b\, l\, \nu$:

isolated lepton with large transverse momentum p_T^l

neutrino $\Rightarrow$ large missing transverse momentum p_T

b-jet $\Rightarrow$ large hadron transverse momentum p_T^{had}

required to suppress W production background

Electroweak cross sections

Single top production

SM cross section below 1 fb^{-1}

FCNC couplings can induce single-top production in several BSM extensions

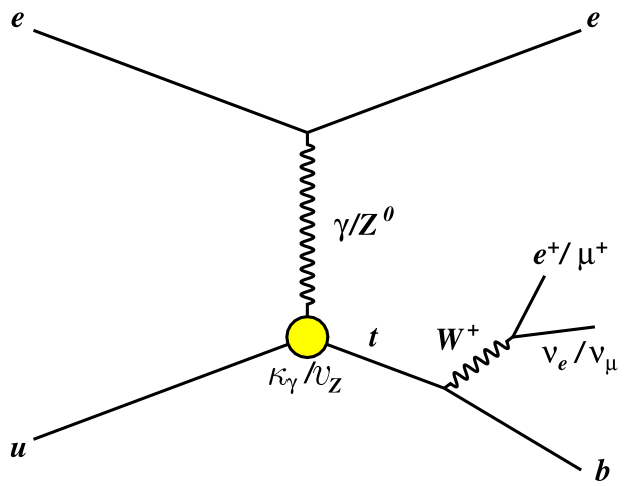

No excess observed

$\sigma < 0.13\ pb$ (95% C.L.)

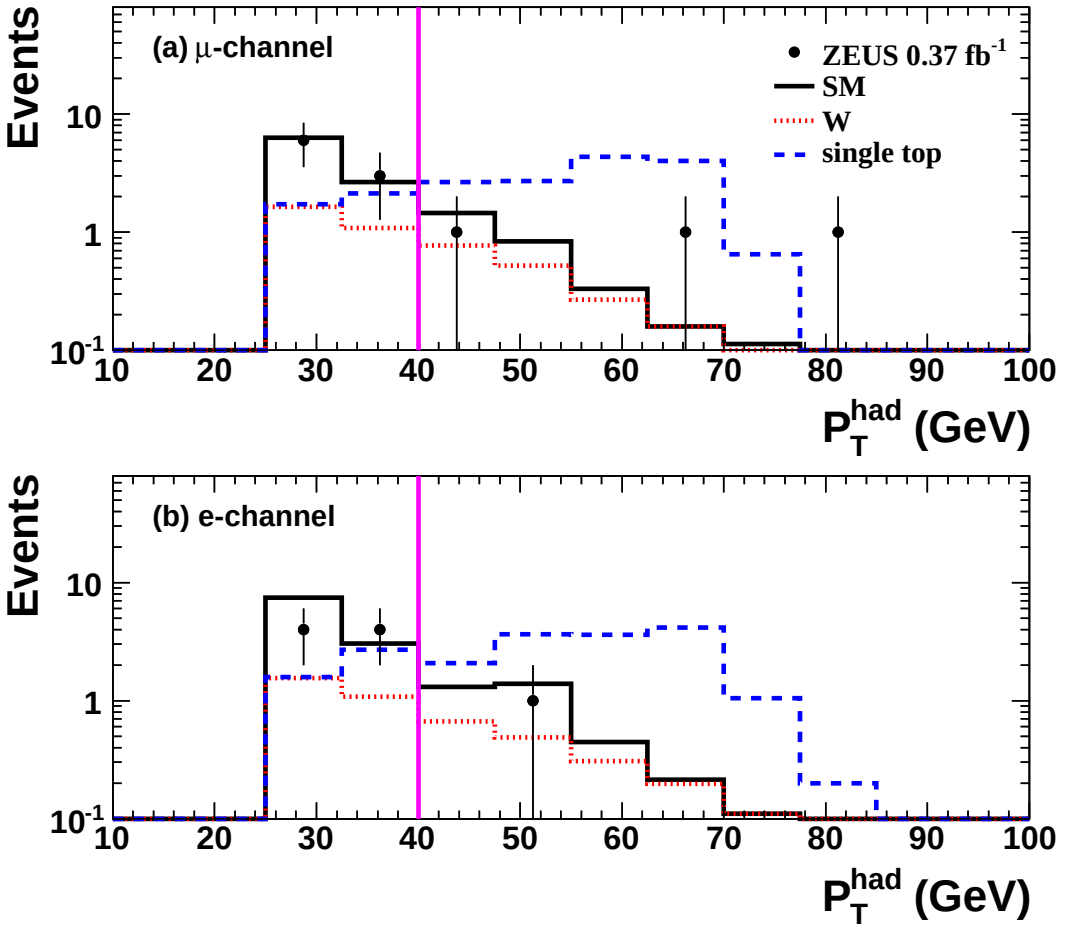

Electroweak cross sections

Single top production

SM cross section below 1 fb^{-1}

FCNC couplings can induce single-top production in several BSM extensions

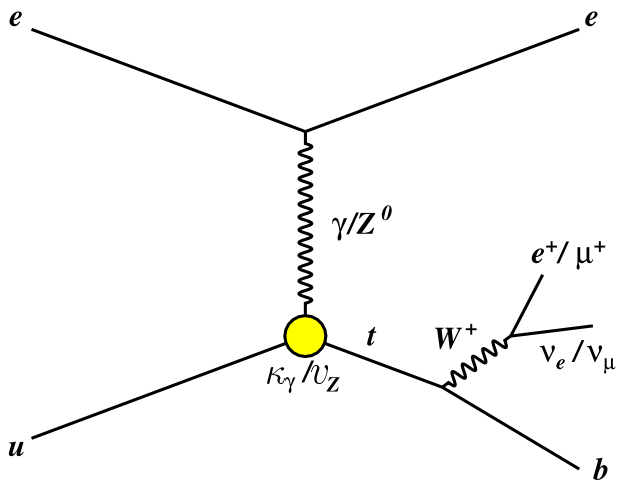

No excess observed

$\sigma < 0.13\ pb$ (95% C.L.)

Resulting constraints on the anomalous top BRs

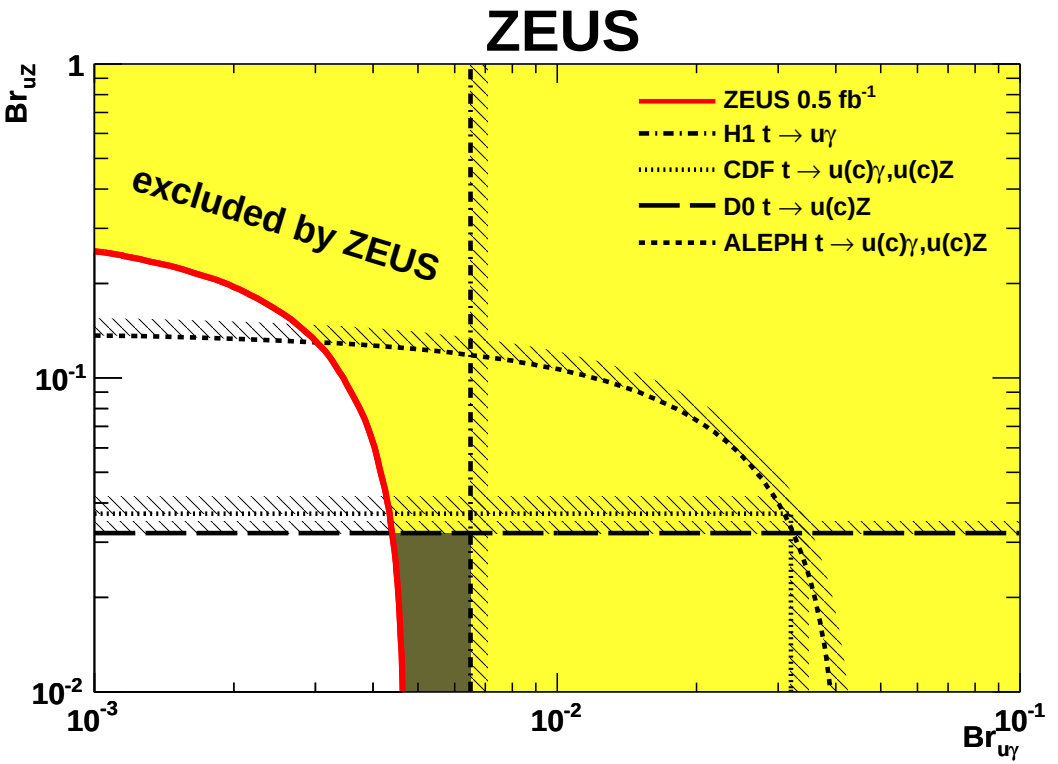

Phys. Lett. B 708 (2012) 27-36

Conclusions

HERA

High luminosity + polarization $\Rightarrow$ unique window for precise EW studies

H1 and ZEUS are finalizing analysis of data collected in 1994-2007

Conclusions

HERA

High luminosity + polarization $\Rightarrow$ unique window for precise EW studies

H1 and ZEUS are finalizing analysis of data collected in 1994-2007

NC and CC DIS at high Q^2 in very good agreement with SM
Including polarization and charge asymmetries

Conclusions

HERA

High luminosity + polarization $\Rightarrow$ unique window for precise EW studies

H1 and ZEUS are finalizing analysis of data collected in 1994-2007

NC and CC DIS at high Q^2 in very good agreement with SM
Including polarization and charge asymmetries

EW parameters can be constrained from HERA data only
No deviations from Standard Model predictions

Conclusions

HERA

High luminosity + polarization $\Rightarrow$ unique window for precise EW studies

H1 and ZEUS are finalizing analysis of data collected in 1994-2007

NC and CC DIS at high Q^2 in very good agreement with SM
Including polarization and charge asymmetries

EW parameters can be constrained from HERA data only
No deviations from Standard Model predictions

Cross sections for W and Z production consistent with expectations
No anomalous single top production observed